


Novel Pseudotaxis Mechanisms Improve Migration of Straight-Swimming Bacterial Mutants Through a Porous Environment

Bitan Mohari,^a Nicholas A. Licata,^{b*} David T. Kysela,^a Peter M. Merritt,^{a*} Suchetana Mukhopadhyay,^a Yves V. Brun,^a Sima Setayeshgar,^b  Clay Fuqua^a

Department of Biology^a and Department of Physics,^b Indiana University, Bloomington, Indiana, USA

* Present address: Nicholas A. Licata, Department of Natural Sciences, University of Michigan-Dearborn, Dearborn, Michigan, USA; Peter M. Merritt, Cytek Development, Fremont, California, USA.

ABSTRACT Bacterial locomotion driven by flagella is given directionality by the chemotaxis signal transduction network. In the classic plate assays of migration in porous motility agar, efficient motility is compromised in chemotaxis mutants of diverse bacteria. Nonchemotactic mutants become trapped within the agar matrix. Suppressor mutations that prevent this entanglement but do not restore chemotaxis, a phenomenon designated pseudotaxis, were first reported to arise for *Escherichia coli*. In this study, novel mechanisms of pseudotaxis have been identified for the plant-pathogenic alphaproteobacterium *Agrobacterium tumefaciens*. Mutants with chemotaxis mutation suppressor (cms) mutations that impart enhanced migration in motility agar compared to that of their straight-swimming, nonchemotactic parent were isolated. We find that pseudotaxis in *A. tumefaciens* occurs most commonly via mutations in the D1 domain of the flagellar hook protein, FlgE, but it can also be found less frequently to be due to mutations in the hook length regulator, FliK, or in the motor protein, MotA. Single-cell-tracking studies of cms mutants in bulk medium clearly reveal frequent changes in the direction of swimming, similar to the swimming of strains that are proficient for chemotaxis, but independent of a sensory mechanism. Our results suggest that the tumbling process can be tuned through mutation and evolution to optimize migration through complex, porous environments.

IMPORTANCE Chemotaxis sensory networks control direct bacterial motility by modulating flagellar rotary motion, alternating cellular movement between runs and tumbles. The straight-swimming phenotype of chemotaxis-deficient cells yields nonexpanding colonies in motility agar. Enhanced, chemotaxis-independent spreading, dubbed pseudotaxis, has been observed in *Escherichia coli* mutants. We have identified novel pseudotaxis mutations in *Agrobacterium tumefaciens* that alter the flagellar hook structure or motor, leading to randomly occurring reorientations observed in single-cell tracking studies in bulk medium. These directional changes allow the cells to migrate more efficiently than the parent strain through the agar matrix, independently of the chemotaxis process. These findings reveal that tumbling can be tuned for effective navigation in complex porous environments, analogous to the natural habitats for many bacteria, and provide evidence for the strong selective pressure exerted by the external environment on the basal pattern of motility, even in the absence of chemotaxis.

Received 2 January 2015 Accepted 7 January 2015 Published 24 February 2015

Citation Mohari B, Licata NA, Kysela DT, Merritt PM, Mukhopadhyay S, Brun YV, Setayeshgar S, Fuqua C. 2015. Novel pseudotaxis mechanisms improve migration of straight swimming bacterial mutants through a porous environment. mBio 6(2):e00005-15. doi:10.1128/mBio.00005-15.

Editor R. John Collier, Harvard Medical School

Copyright © 2015 Mohari et al. This is an open-access article distributed under the terms of the [Creative Commons Attribution-Noncommercial-ShareAlike 3.0 Unported license](https://creativecommons.org/licenses/by-nc-sa/4.0/), which permits unrestricted noncommercial use, distribution, and reproduction in any medium, provided the original author and source are credited.

Address correspondence to Clay Fuqua, cfuqua@indiana.edu.

This article is a direct contribution from a Fellow of the American Academy of Microbiology.

Many bacteria are able to navigate through their local environment using a variety of motility mechanisms. The rotary motion of flagella is utilized by diverse motile bacteria to propel themselves through aqueous media. Flagella are helical extracellular filaments of the protein flagellin that are connected to a flexible curved segment called the hook, anchored to the membrane via the basal body, and powered by a rotary motor complex (1, 2). For *Escherichia coli* and other well-studied bacteria, multiple rotating flagella can coalesce into a multifilament bundle, and the concerted motion of this bundle provides propulsion. In *E. coli*, counterclockwise (CCW) flagellar rotation promotes bundling and drives periods of straight swimming called runs. Clockwise (CW) rotation of one or more flagella leads to polymorphic tran-

sitions of the helical flagellar filament, resulting in bundle disruption that causes reorientations known as tumbles. Although many bacterial species initiate tumbles by reversing flagellar rotation like *E. coli*, others have unidirectional motors, and unbundling occurs when one or more flagella slow their rotation or stop (3–5). For bacteria with multiple flagella, the dynamics and degree of unbundling determine the extent to which the cell is reoriented from its previous course during a tumble (3, 6, 7)

The rotation of the flagellar motor is modulated through its interactions with an intracellular response regulator called CheY that is controlled in turn by the chemotaxis-signaling network. Chemotaxis is a sensory mechanism by which cells bias their movement in response to external chemical gradients. Chemical

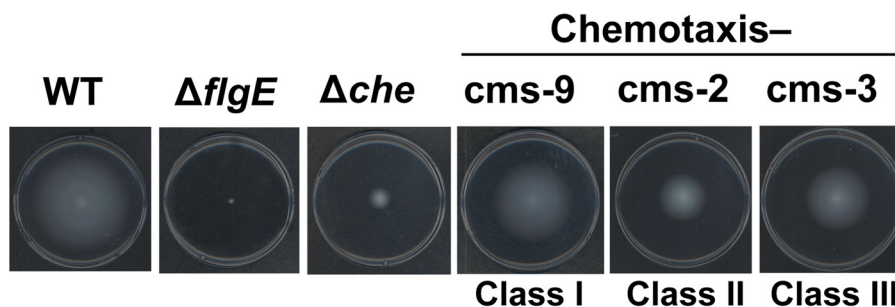


FIG 1 Motility agar phenotypes of one candidate from each class of *cms* mutants. Motility agar images are from day 6. Chemotaxis⁻, class I, II, and III *cms* mutants with deletion of either the entire chemotaxis operon (Δche) or the gene for histidine kinase CheA ($\Delta cheA$); these mutants exhibit identical phenotypes.

signal detection is initiated at receptor clusters in the cytoplasmic membrane and transduced through a complex internal signaling pathway comprised of multiple chemotaxis (Che) proteins (8), culminating in a change in the concentration of phosphorylated CheY (CheY-P). CheY-P stimulates tumbles by binding to the FliM protein in the FliM-FliG-FliN flagellar motor switch complex, which in *E. coli*-type motility systems increases the CW rotational bias. Chemotaxis thereby modulates the frequency of flagellar reversals, regulating the duration of the mean run time and resulting in a biased random walk toward attractants and away from repellents (9–11).

The mechanisms governing the chemotactic response have been intensively studied, and a wide variety of mutants have been isolated. Chemotaxis mutations (e.g., *cheA* mutations) that decrease tumbling frequency lead to relatively straight, uninterrupted runs, whereas other mutations (e.g., *cheB* mutants) can increase tumbling, limiting the frequency and duration of runs. For decades, swimming motility has been assayed using semisolid motility agar (a low-concentration, high-porosity, fluid-filled random network of agarose polymers), by inoculating bacteria at a single point and measuring the radial spread of bacterial growth, the so-called swim ring, over time (12–15). As the bacteria deplete nutrients at the site of inoculation, they establish a chemical gradient, and chemotaxis further promotes the outward radial migration of cells toward higher nutrient levels. For straight-swimming, nontumbling mutants, swim ring advancement is greatly diminished, as cells are impeded by the agar network. Hyperswitching mutants are also less efficient in motility agar migration, as they change direction so frequently that their net movement is compromised. In both cases, decoupling the mean run time from Che control abolishes the ability to bias movement in response to gradients (16–20).

Many of the *E. coli* Che proteins are encoded within the *che* genetic cluster, and *che* cluster deletion mutants are straight swimming and spread inefficiently in motility agar. Extended incubation of an *E. coli che* deletion mutant in these assays was found to generate suppressor mutations that increased the radial spread of the population through the agar, appearing to reverse the chemotaxis deficiency, first shown in a classic work by Wolfe and Berg (21). These secondary mutations were found to give rise to increased tumbling relative to that of the straight swimming parent. Rather than regaining chemotaxis, several of these mutants were found to have elevated flagellar rotation reversals due to point mutations in the *fliM* and *fliG* genes, which encode the flagellar switch and rotor, respectively, and together direct flagellar rever-

sal. While the Che system normally stimulates these reversals, these mutants randomly switch rotation independently (16, 22, 23). Hence, the effective migration of nonchemotactic cells in porous agar, termed pseudotaxis, is a purely diffusive spread of motile bacteria that does not respond to chemical gradients.

Analysis of straight-swimming mutants of the alphaproteobacterial plant pathogen *Agrobacterium tumefaciens* with deletions of the *cheA* chemotaxis regulator or the entire *che* gene cluster led to the isolation of suppressor mutants that rescued the decreased *che* mutant migration through motility agar (24). These were denoted chemotaxis mutation suppressor (*cms*) mutants and were found to have regained the ability to tumble in suspension. The *cms* mutations also resulted in a decreased ability of *A. tumefaciens* to transition from a motile state to a surface-attached biofilm growth mode (24). *A. tumefaciens* produces a sparse tuft of up to 6 polar flagella (25). In contrast to *E. coli* and as with other related members of the *Rhizobiaceae* family, *A. tumefaciens* is thought to drive forward propulsion through CW flagellar rotation, resulting in multifilament bundle formation (4, 26–28). Tumbles are thought to occur due to slowing of CW rotation, causing disruption of the flagellar bundle, rather than through rotation reversal (4, 5, 27). These mechanistic differences suggested that *cms* mutations resulting in *A. tumefaciens* pseudotaxis might not be in the same switch complex components as those in *E. coli*. Indeed, the *fliM* and *fliG* homologues, as well as several motor and *che* gene sequences, were wild type (24).

In this work, we analyze a collection of *A. tumefaciens cms* mutants and utilize whole-genome sequencing to map their mutations. We identify several new mechanisms by which the pseudotaxis phenotype can arise. We find that these mutations affect the structure of the flagellum and the process by which its rotation is powered rather than altering the regulatory switch complex, which can control the speed and direction of flagellar rotation and which is the most common source of pseudotaxis in previous studies on *E. coli* and *Salmonella*.

RESULTS AND DISCUSSION

Alterations in the *A. tumefaciens* flagellar hook result in pseudotaxis. *A. tumefaciens* mutants with chemotaxis mutation suppressors (*cms*) can be readily isolated from cells in flares emanating from the diminished swim ring of straight-swimming Che mutants (e.g., $\Delta cheA$ mutants or mutants with deletion of the entire Che cluster [Δche], Atu0514 to Atu0522) after extended incubation on motility agar. Such *cms* mutants exhibited extended swim rings (Fig. 1; Fig. S1A and C in the supplemental

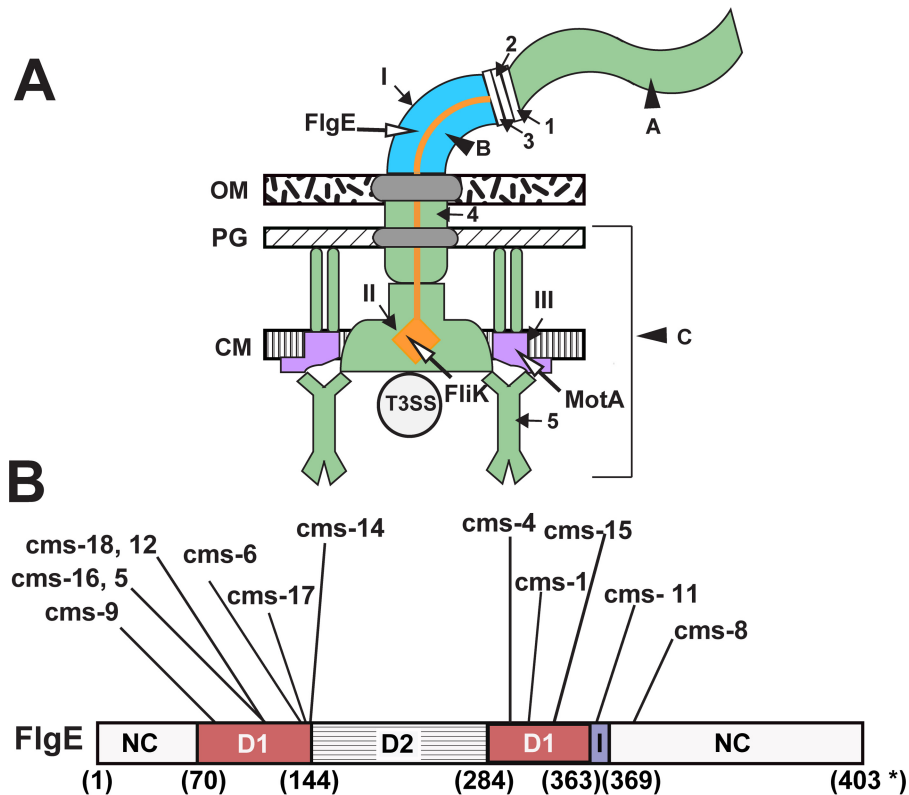


FIG 2 Flagellar structure with cms mutations and FlgE domain organization. (A) Flagellar structure. Black arrowheads denote flagellar substructures, i.e., the filament (A), hook (B), and basal body (C). Roman numerals I, II, and III indicate mutations as follows: class I (FlgE), blue; class II (FliK), orange; class III (MotA), purple. Flagellar proteins whose genes were found to be wild type by direct sequencing are indicated by numbers 1 to 5 as follows: 1 and 2, hook filament junction proteins FlgK and FlgL; 3, hook cap protein FlgD; 4, distal rod protein FlgG; 5, switch protein FliM. FliK is drawn as an extended filament that runs from the basal body through the hook. (B) Domain organization based on the *Salmonella* FlgE structure. Approximate boundaries are indicated, and lengths in amino acids are shown under the bar. NC, protein segments (1 to 70 and 370 to 402) that were not crystallizable; I, a region that is invisible in the electron density map (364 to 369). Locations of class I cms mutations in the two regions that comprise domain D1 are indicated, corresponding to the data in Table 1. D2 is the outer domain (30, 68). The *Salmonella* FlgE is 403 aa, while *A. tumefaciens* FlgE is 425 aa, and this difference is denoted by an asterisk in the figure.

material) and tumbling swimming in suspension, in contrast to the small swim ring and straight swimming of their parent strain. Although these mutants were phenotypically similar to the pseudotaxis mutants of Wolfe and Berg (21), the *fliM* and *fliG* genes, encoding the switch and rotor, were wild type in the *A. tumefaciens* cms-1 mutant. Whole-genome sequencing the cms-1 mutant, using Illumina high-throughput sequencing, indicated a single base substitution (C1010G) within the 1,278-bp *flgE* (Atu0574) gene encoding the flagellar hook (Fig. 2A), resulting in a change from alanine to glycine (A337G) (Fig. 2B; Table 1). Fifteen more cms mutants were independently isolated from *A. tumefaciens cheA* and *che* mutants in two separate screens for suppressors on motility agar. Independent cms mutants were designated with numerical suffixes (Table 1). Twelve of these had mutations in *flgE*, 11 had single missense mutations, and cms-15 had incurred an 18-bp base duplication. All of these cms mutants were independent, but two pairs had identical mutations (cms-5 and -16 and cms-12 and -18) (Table 1). We designated the *flgE* alleles class I cms mutants.

Class I cms mutations map to the FlgE D1 domain. We next mapped the cms mutations onto the hook structure. The three-dimensional structure of the *A. tumefaciens* FlgE protein (FlgE_{At}) has not been determined; however, the structure of the related *Salmonella enterica* serovar Typhimurium FlgE (FlgE_{ST}) is avail-

able, and the amino acid sequences of the two proteins are 31% identical and 46% similar. X-ray crystallographic and cryo-electron microscopy (cryo-EM) studies determined that FlgE_{ST} consists of four unique domains (Fig. 3A and B) (29, 30), D0, D1, D2, and Dc. The D1 domain (residues 71 to 144 and 285 to 363) is the central domain, flanked on one side by an alpha-helical coiled-coil formed by D0 (residues 1 to 24 and 367 to 402) and Dc (residues 25 to 70) and on the other side by a flexible linker, followed by the D2 domain (residues 145 to 284). The D0 and Dc domains are closely packed in the hook interior, while the D1 and D2 domains are external to the hook central axis (Fig. 3B). We aligned the FlgE_{At} and FlgE_{ST} amino acid sequences (see Fig. S2A in the supplemental material) (31), mapping the cms FlgE_{At} mutations onto the homologous positions in the FlgE_{ST} structure (PDB ID 3A69) (29). Nine of the 11 class I cms mutations we identified clustered together on one face of the central D1 domain (Fig. 3A). For the cms-14 mutation, there was no corresponding FlgE_{ST} residue, and for the cms-15 mutation, the six additional duplicated amino acids could not be modeled (32, 33).

The arrangement and interaction of the ~120 FlgE monomers that make up the hook are critical to its function. The flexibility of this highly ordered, helical complex has been shown to be important for proper flagellar rotation, bundling, and unbundling (34, 35). We hypothesize that the class I cms mutations in *flgE*, through

TABLE 1 Mutations and phenotypes of cms mutants

Mutant	Gene product	Base mutation	Amino acid change	Swim ring size (% of WT \pm SEM)	Biofilm biomass (% of WT \pm SEM)
Δche mutant	NA ^c	NA	NA	33.3 \pm 1.7	182.4 \pm 7.6
cms-1	FlgE	C1010G	A337G	84.4 \pm 0.6	51.3 \pm 8.8
cms-2	FliK	G1275 deletion	FliK-Atu0572 fusion (620 aa)	50.6 \pm 1.5	28.0 \pm 3.6
cms-3	MotA	C536G	A179G	55.6 \pm 1.1	49.3 \pm 2.0
cms-4	FlgE	G955C	G319R	68.9 \pm 1.1	47.4 \pm 3.5
cms-5	FlgE	A380G	Y127C	80.6 \pm 2.0	29.5 \pm 2.8
cms-6	FlgE	G412T	V138F	82.8 \pm 0.6	28.7 \pm 4.3
cms-8	FlgE	G1115A	G372D	42.8 \pm 0.6	25.5 \pm 6.0
cms-9	FlgE	G277T	V93F	82.2 \pm 2.9	75.6 \pm 8.5
cms-11	FlgE	T1102C	F368L	81.1 \pm 3.1	34.8 \pm 5.7
cms-12	FlgE	A380C	Y127S	86.7 \pm 2.5	28.4 \pm 2.8
cms-14	FlgE	T431C	L144P	81.1 \pm 1.5	ND ^d
cms-15	FlgE	Duplication of bases 1063–1080 (TATCTGCCGAGCAACGAC)	Duplication of aa 355–360 (Y-L-P-S-N-D)	72.2 \pm 0.6	ND
cms-16	FlgE	A380G	Y127C	ND	ND
cms-17	FlgE	G428A	G143D	85.6 \pm 1.1	ND
cms-18	FlgE	A380C	Y127S	ND	ND
cms-19	FliK	Stop codon (TGA) mutated to CGA	FliK + 12 aa	56.1 \pm 0.6	ND

^a Swim ring values are from 168 h.

^b Biofilm values are from 72 h postinoculation.

^c NA, not applicable.

^d ND, not determined.

changes in the hook structure and/or flexibility, alter nominal flagellar bundling, causing the cms mutant cells to tumble. One possibility could be that these mutants develop shorter or longer hooks. However, transmission electron microscopy (TEM) analysis of class I cms mutant hooks revealed no obvious differences in length (Fig. 4B). In order to evaluate how the altered FlgE residues in cms mutants might interact between adjacent monomers, FlgE subunits were modeled into the hook structure, based on images of chemically straightened hooks from *S. Typhimurium* (29, 36). Each turn of the helical hook structure consists of 11 FlgE monomers (Fig. 3B). No predicted intermolecular interactions are revealed between the mutated cms residues and other monomers within one helical turn, but in the assembled straight-hook model, FlgE monomers in one helical turn are in close proximity to monomers in an adjacent helical turn (Fig. 3C). Specifically, resi-

dues V93 in cms-9 and Y127 in cms-12 interact with D2, and G372 in cms-8 interacts with D1 of an adjacent FlgE monomer. The distance between the cms mutations and their nearest neighboring residues is 12 Å, precluding specific electrostatic or hydrophobic interactions between individual monomers in the straight-hook model. In a dynamically bending hook, these distances are likely to change, making transient short-range interactions between the helical rings possible as the hook isomerizes in its function as a universal joint. We hypothesize that the cms FlgE proteins modify the dynamic interactions within the hook structure, ultimately altering flagellar motion and promoting frequent unbundling of the flagella.

Pseudotaxis due to mutations in the FliK hook length regulator and the MotA flagellar motor protein. Several less frequent cms mutants did not have mutations in *flgE* or any of several other

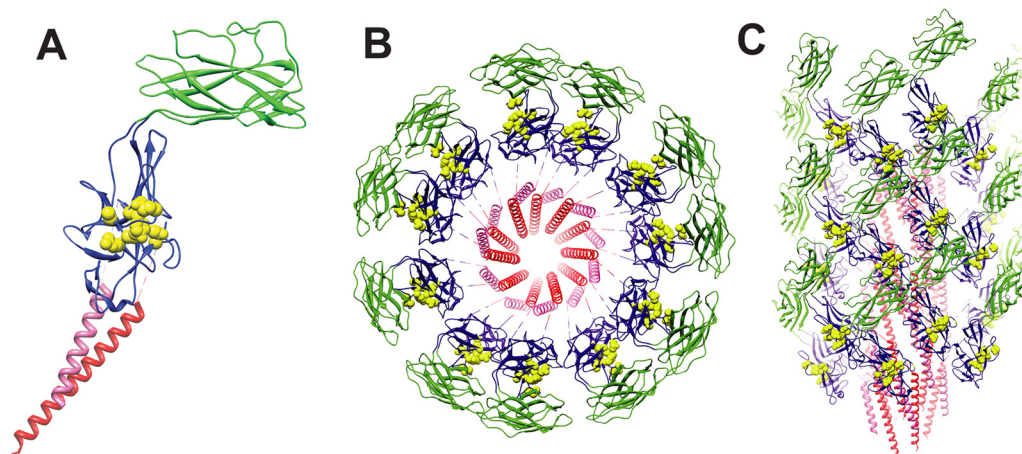


FIG 3 cms mutations modeled onto the *S. Typhimurium* FlgE protein and hook. (A) The monomeric FlgE domains determined from the cryo-EM structure are color coded as follows: D0, pink; D1, blue; D2, green; Dc, red. The cms mutation sites are shown as yellow space-filling models. (B) One helical turn of the straight hook composed of 11 FlgE monomers. (C) A side view of four helical turns in the straight-hook model.

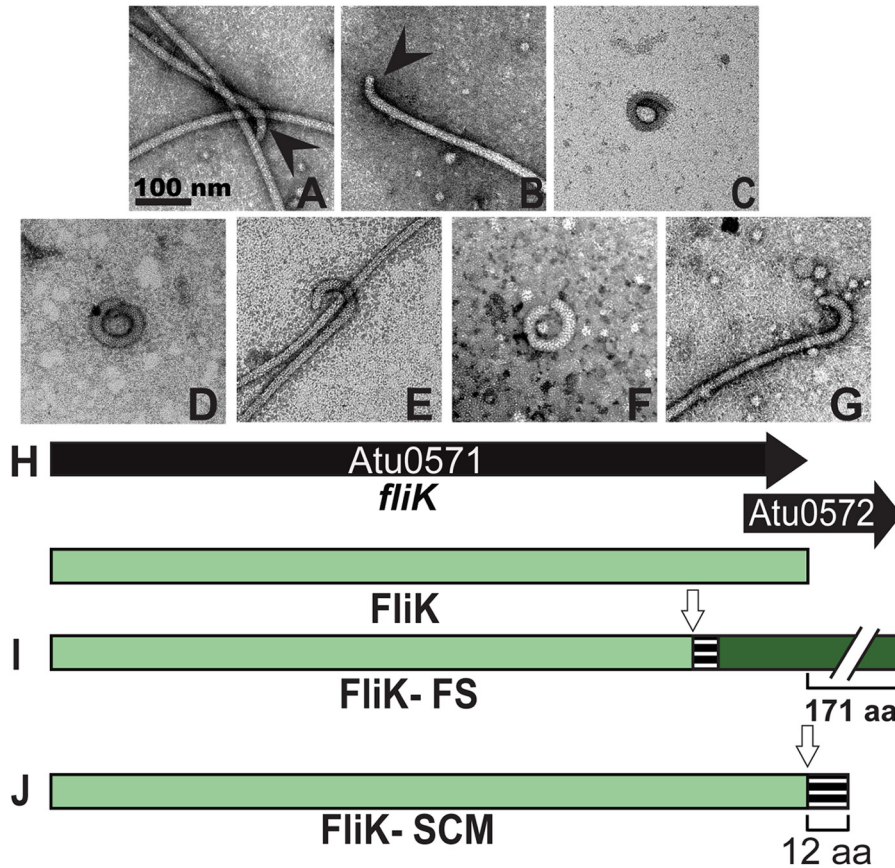


FIG 4 Flagellar hook morphologies of *cms* mutants, organization of *fliK* locus, and FliK mutant variants. (A to G) TEM images with uranyl acetate staining of wild-type filaments showing the hook (black arrowhead) (A), class I *cms* (*flgE*) mutant showing a normal hook (black arrowhead) (B), coiled polyhooks in a $\Delta fliK$ mutant (C), and polyhook and polyhook filaments in class II mutants *cms-2* (D and E) and *cms-19* (F and G). The scale bar in panel A applies to all TEM images. (H) Gene organization of *fliK* and the overlapping (17 bp) downstream gene *Atu0572*, shown as solid black arrows, and FliK polypeptide, shown as a light green bar. (I) White arrow indicates the position of the single-base frameshift (FS) in *fliK* *cms-2* that alters the polypeptide sequence, resulting in the 620-aa FliK-FS polypeptide. The striped region indicates the 8 out-of-frame amino acid residues that are followed by the *Atu0572* polypeptide (dark green). (J) White arrow indicates the stop codon mutation (SCM) in *fliK* *cms-19* that extends the polypeptide by 12 aa residues, indicated by the striped region, to produce a 461-aa FliK-SCM polypeptide.

flagellar structural genes that were sequenced. Whole-genome sequencing revealed that the *cms-2* mutant had incurred a single-base deletion mutation at position 1275 of the *fliK* gene (Atu0571), encoding the putative hook length regulator (37). The deletion resulted in a frameshift within the 3' region of *fliK*, thereby extending the native 449-amino acid (aa) gene product to 620 aa (Table 1). This frameshift mutation fuses *fliK* in frame to the downstream *Atu0572* coding sequence (a putative lytic transglycosylase), the 5' end of which overlaps the *fliK* 3' end by 17 bp, thus resulting in a FliK protein that is fused to 8 out-of-frame amino acids and the entire *Atu0572* translation product (Fig. 2A and 4I). An additional *cms* derivative was also due to a *fliK* mutation in which the native stop codon is altered (*cms-19*, TGA to CGA), extending the coding sequence by 12 codons and producing a 461-aa mutant FliK protein (Fig. 4J). We designated these non-*flgE* *cms* isolates class II (*fliK*) mutants.

The two class II *cms* mutations extend the *fliK* coding sequence and are predicted to produce a longer FliK protein (Fig. 4I and J). FliK functions in the determination of the flagellar hook length, and mutants with null mutations of *fliK* in *Sinorhizobium meliloti*, a close relative of *A. tumefaciens*, produce abnormally large and

aberrant flagellar hook structures called polyhooks (37). We therefore compared the flagellar structures of class II mutants to the structures of the wild type and an *A. tumefaciens* *fliK* deletion mutant using TEM. Wild-type hook structures are only occasionally visible as small bulbs of material at the end of sheared or dislodged flagellum filaments (Fig. 4A). The deletion of *fliK* in *A. tumefaciens* results in nonmotile derivatives that shed large coiled structures of ≥ 200 nm, readily visible using TEM, that we define as polyhooks (Fig. 4C). The two class II mutants *cms-2* and *cms-19*, with mutations that encode C-terminally extended FliK proteins, produce large, readily visible filaments with much more heterogeneous structures, some coiled, some with extended polyhook filaments, and some normal flagella (Fig. 4D to G). However, in contrast to the *fliK* deletion mutants, these mutants are motile and, therefore, must generate functional flagella. The FliK C terminus is thought to interact with the FlhB protein in the basal body in order to switch from hook assembly to filament assembly (38). The class II mutations may reduce the efficiency of this switching process, fostering the formation of polyhooks and polyhook filaments. As with class I mutants, alteration of the hook structure is likely to

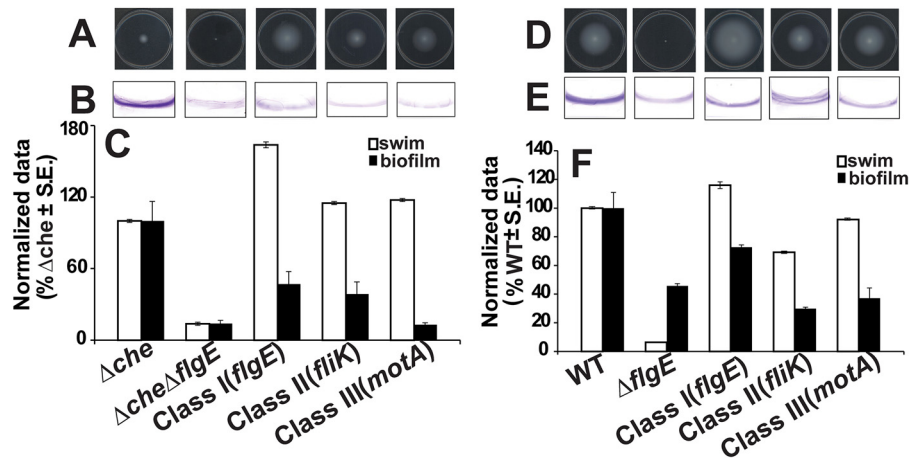


FIG 5 Motility assays and static culture biofilm formation for derivatives with cms mutant alleles. Results are shown for mutants with cms mutations in the Δche mutant background (A, B, and C) and in the wild-type background (D, E, and F). (A and D) Motility assay plates of cms mutants after 6 days of incubation. (B and E) Coverslip biofilms at 48 h. (C and F) Swim ring diameters measured after 7 days (white bars), and amounts of solubilized crystal violet (33% acetic acid) normalized to culture turbidity (A_{600}/OD_{600} ratio) from coverslip biofilm assays (black bars). $\Delta che \Delta flgE$ and $\Delta flgE$ mutants are the nonmotile and attachment-deficient controls. Images of representative motility plates at 6 days of incubation are shown above the corresponding bars. All measurements are normalized to the data for the parent Δche mutant (C) and the wild type (F); error bars show standard errors of the mean results of three independent experiments.

impede flagellar bundling, leading to tumbles in an otherwise straight-swimming background.

In contrast to the *fliK* mutations, the cms-3 mutant had a single base substitution (C536G) in the *motA* gene (873 bp, Atu0560), encoding a mutated (A179G) flagellar motor protein (Fig. 2A; Table 1; Fig. S2B in the supplemental material). This non-*flgE* cms isolate was designated a class III (*motA*) cms mutant. All of the cms mutants exhibited more efficient swim ring expansion than their Che^- parents (Fig. 1; Table 1). We introduced the identified mutations into a naive background by allelic exchange for representative class I, II, and III mutants in the *A. tumefaciens* Δche mutant, and the swimming deficiency was suppressed in these derivatives, as with the isolated cms mutants (Fig. 5A and C; Fig. S1A and C).

cms mutants exhibit random and erratic swimming behavior. Comparisons of the swimming behavior of cms mutants with that of wild-type *A. tumefaciens* and other derivatives by single-cell microscopic tracking of cells in suspension were performed. Wild-type *A. tumefaciens* exhibits periodic switching between runs and sharp directional changes or turns (Fig. 6A), whereas the Δche mutant shows markedly smooth swimming behavior (Fig. 6B). Representatives of the three different cms mutant classes were examined in parallel: mutants in class I (cms-9 [FlgE V93F]), class II (cms-2 [FliK frameshift]), and class III (cms-3 [MotA A179G]) all exhibit notably discontinuous motion, with clear runs and abrupt reorientations or directional changes (Fig. 6C to E). This swimming behavior is consistent with the tumbly phenotype observed for the cms-1 (FlgE A337G) mutant under light microscopy (24).

Single-cell trajectories were tracked using the particle tracker plug-in of the Fiji image analysis package (39, 40). Trajectory plots were obtained by utilizing a MatLab program developed by our group. We examined at least 20 separate trajectories for class I, II, and III representatives (see Materials and Methods for details on tracking analysis). The number of reorientations made by the cell over time was manually recorded from the single-cell traces by eye, and the swimming speeds were calculated from the trajectory reports generated by the particle tracker. The Δche parent strain

exhibited virtually no reorientations in an unobstructed aqueous environment (other than a gradual change in direction due to rotational Brownian motion) and a high swimming speed relative to that of the wild type (median value of $\sim 46 \mu\text{m/s}$ compared to $\sim 29 \mu\text{m/s}$) (Fig. 6F and G). The cms mutants exhibited significantly higher reorientation frequencies relative to that of their Δche parent, comparable to that of the wild type, with the class III *motA* mutant being the least tumbly (in comparison to the results for the wild type, the P value was <0.01) (Fig. 6F).

The swimming speeds for class I and class II mutants did not differ significantly, but the class III *motA* mutant was slower than the wild type (median value of $\sim 17 \mu\text{m/s}$; $P < 0.0001$) (Fig. 6G). The same *motA* mutation in the wild-type background also resulted in a similar slower swimming speed (median value of $\sim 18 \mu\text{m/s}$; $P < 0.0001$). In *S. meliloti*, coordination between Arg90 and Glu98 of MotA is important for chemokinesis (control of speed modulation) and Glu150 is important for torque generation (5). The alanine residue that is mutated in cms-3 (MotA A179G) is in this region and is conserved in *E. coli* MotA (see Fig. S2B in the supplemental material) but is of unknown function. This segment of MotA is predicted to be helical, and glycine residues are known to disfavor helix formation (41). The FliG rotor protein interacts with this region of the MotA motor protein, and the slower swimming speed of cms-3 (Fig. 6G) may be due to a decreased rate of flagellar rotation. This alteration in the flagellar rotation rate was shown in numerical studies to compromise flagellar bundling, likely leading to the tumbles observed in these mutants (42).

cms alleles affect motility even in strains proficient for chemotaxis. The cms mutants were isolated from straight-swimming, chemotactically deficient parents. Wild-type *A. tumefaciens* Che^+ derivatives engineered to harbor cms mutations were evaluated for motility and biofilm formation. Interestingly, the class I cms (*flgE*) allele moderately but significantly enhanced migration efficiency compared to that of the wild type (Fig. 5D and F). We hypothesize that this is due to the additive effect of chemotaxis and the activity of the altered cms hook that promotes more efficient

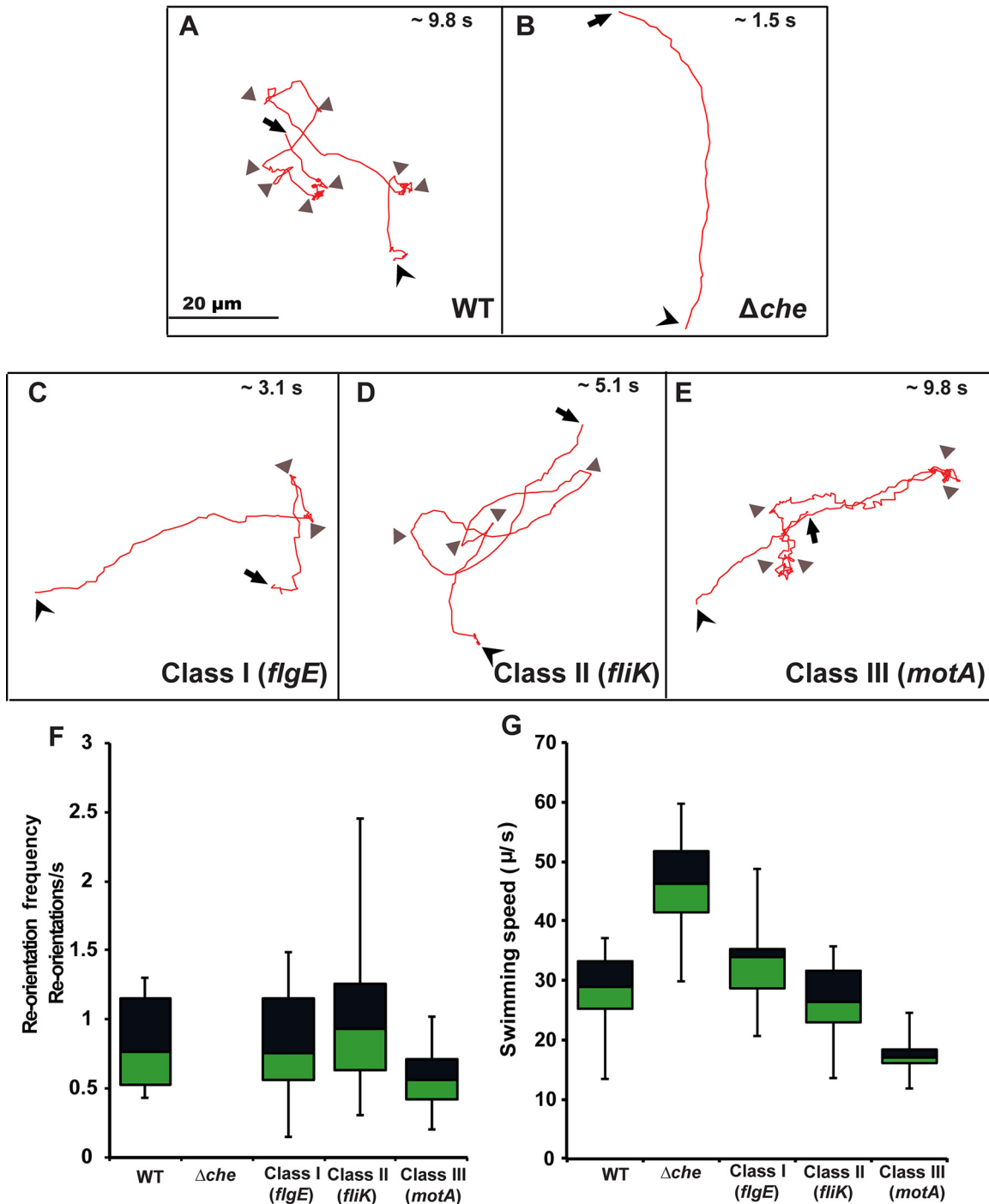


FIG 6 Tracking of actively motile cells and determination of swimming metrics. (A to E) Examples of swimming trajectories for the wild type and the indicated mutants. Black arrowheads indicate trajectory starts, and black arrows indicate termini. Gray triangles indicate reorientation of the cell. The time scale for each trajectory is indicated. The scale bar in panel A applies to all trajectories. (F and G) Box plots presenting the quantified reorientation frequencies and swimming speeds: lines denote median values, boxes give the interquartile range, and bars indicate highest and lowest values. Reorientations were considered to be events that changed the overall direction of movement. The *Δche* mutant has a reorientation frequency of 0 and therefore has no data in panel F. Swimming speed includes the time during reorientations.

expansion through the agar matrix. The class II cms (*fliK*) mutation compromises the motility agar phenotype in a wild-type background (Fig. 5D and F). The class III cms (*motA*) allele exhibited only a modest decrease relative to that of the wild type

(Fig. 5D and F). These mutant phenotypes clearly indicate that the characteristics of the original cms isolates were the net effect of the chemotaxis deficiency and the changes to flagellar function caused by the cms mutation combining to improve migration through

motility agar. The ability to perform chemotaxis improves motility even with these additional flagellar mutations.

Complementation of cms mutants: tests for dominant-negative effects. The original cms mutations were haploid. It seemed possible that the cms mutations in merodiploids would be dominant over the wild-type copies of the mutated genes (*flgE*, *fliK*, and *motA*). Plasmid-borne expression of the *flgE*, *fliK*, and *motA* cms alleles from the *lacZ* promoter (P_{lac}) in otherwise wild-type *A. tumefaciens* cells that have chromosomal copies of the corresponding genes did not result in any notable decrease in motility, even at the strongest level of induction (see Fig. S3A and B in the supplemental material). Conversely, plasmid-borne copies of the *flgE* and *motA* wild-type alleles expressed from P_{lac} decreased the motility of the corresponding cms mutants to levels similar to that of the Che^- parent (Fig. S3C and D). This suggests that the *flgE* and *motA* cms alleles are recessive to the wild-type genes, perhaps indicating modest deficiencies that favor the incorporation and/or functions of the nonmutated proteins over the mutant proteins.

Both of the class II cms mutations were different from the class I and class III mutations in that the frameshift and the stop codon mutations in the *fliK* gene are likely to affect the expression of the downstream gene *Atu0572*. These mutations would disrupt the translation initiation of the overlapping *Atu0572* start codon, 14 bp upstream from the *fliK* stop codon. The plasmid-borne *fliK* gene weakly complemented the cms-2 mutant, and plasmid-borne expression of *Atu0572* alone had no effect (see Fig. S3E and F in the supplemental material). However, a plasmid with both genes (P_{lac} *fliK*-*Atu0572* fusion) in their native configuration achieved nearly full complementation, suggesting that disruption of *Atu0572* expression in the class II cms-2 mutant contributes to the strength of its suppressor phenotype (Fig. S3C and D). The *Atu0572* gene product has homology to lytic transglycosylases and, thus, might be involved in the remodeling of peptidoglycan during assembly of the flagellum.

We also investigated whether the cms-2 fusion product between *fliK* and *Atu0572* could function *in trans* to complement a *fliK* mutant. The plasmid-expressed *fliK*-*Atu0572* fusion (P_{lac} *fliK*_{cms-2}-*Atu0572*) complemented the nonpolar, in-frame Δ *fliK* mutant nearly as well as these same two genes in their wild-type, independent organization expressed from the identical plasmid (P_{lac} *fliK*-*Atu0572*) (see Fig. S4A and B in the supplemental material). The Δ *fliK* mutant was also complemented by the plasmid-borne expression of a wild-type copy of *fliK* alone (P_{lac} *fliK*) (Fig. S4C and D). These findings suggest that the *fliK*-*Atu0572* fusion product functions nearly as well as the wild-type FliK protein and are consistent with the original motile phenotype of the cms-2 mutant, in contrast to that of a *fliK* null mutant.

cms mutations have nonadditive effects on motility. We hypothesize that the cms mutations alter flagellar behavior and bundling sufficiently that they improve the migration of the Che^- parents through motility agar, but not to the extent that they dramatically inhibit motility. This would predict that the presence of multiple cms mutations within the flagellar hook and between the hook and MotA motor protein would not be additive in their effect on motility and, in combination, might even diminish the rate of migration through motility agar. A mutant with two class I cms mutations in FlgE—V93F (cms-9) and Y127C (cms-5)—was created by allelic replacement with a mutagenic plasmid carrying both the cms-5 and the cms-9 mutation, which was utilized to

modify the initial Δ *che* cms-9 mutant. The combined mutations (class I_{cms-9} + I_{cms-5}) resulted in a motility agar phenotype indistinguishable from that of the original mutants (see Fig. S5 in the supplemental material). This indicates that these mutations are nonadditive and that the flagellar hook is able to tolerate multiple and different cms mutations. To create combinatorial mutations of the FlgE flagellar hook protein and the MotA protein, class I and class III alleles were combined. We generated a mutant which combined the FlgE V93F (cms-9) mutation with the MotA A179G mutation by allelic exchange of the cms-9 *flgE* mutation into the initial Δ *cheA* cms-3 mutant (class I_{cms-9} + III_{cms-3}). The combined mutations did not additively enhance the pseudotaxis phenotype, and in fact, the mutant was at least as debilitated as the original cms-3 mutant (Fig. S5). These observations are again consistent with the specificity of the cms mutations, which have independently satisfied the selection for enhanced migration through swim agar.

Biofilm deficiencies of cms mutants. In addition to a tumbling phenotype and enhanced migration through swim agar, the original cms-1 mutant (FlgE A337G) was severely compromised in surface attachment and biofilm formation relative to those of its Δ *cheA* parent and the wild type. The provision of a plasmid-borne *cheA* gene that fully complements the Δ *cheA* mutation did not correct this attachment deficiency (24). This indicated that the cms-1 biofilm deficiency was not a combinatorial effect of both the *cheA* and *flgE* mutations but, rather, was specifically due to the change in *flgE*. In fact, all classes of cms mutants exhibited diminished surface interactions (Table 1; see Fig. S1B and C in the supplemental material). Given recent work on the role of the motor assembly in mechanosensing (43), our results are consistent with the flexibility of the hook playing a role in surface detection and the subsequent engagement of attachment processes. Alternatively or perhaps in addition to this, the uncontrolled and more erratic swimming motion of cms mutants might physically preclude productive surface interactions. All of the cms mutations diminished biofilm formation in both a Che^- background and an otherwise wild-type strain (Fig. 5B, C, E, and F).

Conclusions. In the alphaproteobacterium *A. tumefaciens*, we have identified spontaneous mutations that restore effective tumbling in straight-swimming chemotaxis-deficient mutants to approximately the level in the wild type via mechanisms that are distinct from those previously identified in enteric bacteria (21–23). In contrast to mutations in the flagellar switching mechanism as previously described, these mutants alter the tumbling propensity through structural changes to the flagellar hook and through a change to the MotA motor protein that drives the rotation of each flagellum. These mutants are also deficient in attachment to surfaces, possibly due to impairment of flagellum-mediated surface sensing mechanisms.

For bacteria with multiple flagella, the formation and stability of the flagellar bundle are major determinants of swimming behavior, and bundle disruption causes reorientation of the cell. Reigh et al. (7) computationally investigated the stability of a flagellar bundle by modeling *Agrobacterium* sp. strain H13-3 (highly related to *Agrobacterium tumefaciens*) with 5 to 10 peritrichous flagella and a mesoscale hydrodynamics simulation method for the fluid. This and other studies suggest that unbundling events and the resulting cellular tumbles are due to differences in the torque generated from individual flagellar filaments and their organization relative to each other on the cell surface (3, 7, 44).

Simulation predicted that hydrodynamic interactions between flagella, short-range volume exclusion, and flagellar flexibility are key physical factors governing their synchronization and bundling. For small differences in adjacent motor torques, bundle formation was robust, but as the torque difference was increased, a flagellar phase lag occurred, followed by intermittent slippage and, finally, unbundling. The *cms* mutations isolated in this study generate tumbles in otherwise straight-swimming mutants through alterations that affect the universal joint and the hook and through mutation of the motor. Thus, while the chemotaxis-deficient mutants are trapped in the agar matrix and cannot make the directional changes to escape, the *cms* mutants apparently overcome this barrier via reorientation and, hence, exhibit expansion and improved migration. Our work suggests that the class I (hook) and class II (hook length regulator) mutations generate tumbles by altering the dynamics of flagellar bundling. Mutations in the *MotA* protein of the related *Agrobacterium* sp. H13-3 have been reported to slow flagellar rotation and to cause motility to be so jiggly that migration through motility agar is compromised (45). The class III *motA* mutant we identify here may cause a less dramatic but related modification of the motility apparatus, whereby a decrease in the rate of flagellar rotation alters bundling, leading to sufficient tumbles to facilitate migration through motility agar.

Why did selection for increased migration through motility agar in *A. tumefaciens* result in mutations that alter the hook or motor proteins, presumably altering the mechanical properties of the flagellum, whereas the identical selection in *E. coli* yielded regulatory mutations in the switch complex? No switch mutants were identified in the *A. tumefaciens* screen, and no hook or motor protein mutants were obtained in the *E. coli* studies (21–23). We hypothesize that this reflects the profound mechanistic differences between motility systems that generate tumbles through reversal of flagellar rotation, as in *E. coli* (1), and systems that slow or stop unidirectional rotation to induce tumbles (3). The polar arrangement of flagella in *A. tumefaciens*, in contrast to a peritrichous organization, may also contribute to differences in the details of the bundling and unbundling processes that govern transitions between runs and tumbles and associated tumble angle distribution. The related bacterium *S. meliloti* has a peritrichous flagellar organization, and despite extensive studies examining its chemotaxis (46, 47), including analysis of straight-swimming mutants, the suppression observed for the *A. tumefaciens* *cms* mutants described here has not been reported.

Our findings point to the importance of the tumbling process in navigating complex environments. Even in the absence of a chemotactic response, the intrinsic tumbling rates and tumble angle distributions are likely to be evolutionarily adapted for enhanced performance under specific conditions. Chemotaxis acts to modulate this basal reorientation rate to provide directionality to motility. It seems certain that natural selection has acted upon these properties for each specific bacterial system and that the basal flagellar dynamics are to some extent optimized for the habitats in which these bacteria evolve.

The intense selective pressure exerted in motility agar, in which those bacteria that can better migrate outwards experience a significant growth advantage, made it possible to isolate apparent suppressor mutants of diminished migration resulting from disabled chemotaxis. Indeed, recent work has highlighted the difference in chemotactic behavior in liquid medium versus agar from

the standpoint of optimal concentrations of chemotaxis proteins (CheR and CheB) determining the adaptation rate and tumbling frequency (48). These strong selective pressures are likely recapitulated in natural environments, with heterogeneous distributions of chemical stimuli and complex microarchitecture. While most bacteria in which motility has been studied appear to be chemotactic (49), it has been suggested that organisms may separate motility from the chemotaxis system (50). In the evolutionary path from motility to directed cell movement under the control of a sensory network, an intriguing point that our work highlights is that environments of different porosity provide strong selection for specific reorientation dynamics, and this evolutionary tuning of basal motility almost certainly provides the ground state on which chemotaxis developed.

We observe that the *cms* mutations, in contrast to their positive effect on migration through motility agar, have a uniformly detrimental impact on surface colonization and biofilm formation. Many bacteria, including *A. tumefaciens*, undergo a complex physiological acclimation to contact with surfaces, such as the production of alternative flagellar systems and adhesin production (51, 52). Indeed, as bacteria get close to surfaces, the dynamics of flagellar rotation can dictate the pattern of interactions (53). While it is known that flagella drive surface colonization through the promotion of collisions with surfaces and, in some cases, by acting directly as adhesins (24, 54), the mechanisms underlying surface detection in bacteria—likely mediated by flagella in some cases—are as yet poorly understood. The *cms* mutations, with the resulting compromised surface attachment, appear to disrupt the normal surface acclimation process. High-resolution microscopic comparison of these mutants at surfaces would provide insights into the mechanistic basis for their adhesion deficiency and, more generally, the biophysical mechanisms underlying surface detection.

MATERIALS AND METHODS

Bacterial strains, plasmids, and growth conditions. The bacterial strains, plasmids, and oligonucleotides used in this study are listed in Table S1 and S2, respectively, in the supplemental material. Oligonucleotide primers were obtained from Integrated DNA Technologies (Coralville, IA). DNA was manipulated as described previously (55), and DNA sequencing was performed on an ABI 3730 sequencer at Indiana Molecular Biology Institute, Bloomington, IN. DNA purification was done using E.Z.N.A. plasmid miniprep kits (Omega Bio-Tek, Norcross, GA). All restriction enzymes and molecular biology reagents were obtained from NEB (Ipswich, MA). Electroporation to introduce plasmids into *A. tumefaciens* was performed as described previously (56, 57). *E. coli* was grown in LB medium, and *A. tumefaciens* was grown in AT minimal medium (58) supplemented with 0.5% (wt/vol) glucose and 15 mM ammonium sulfate (ATGN). For *sacB* counterselection, 0.5% sucrose was used as the sole carbon source (ATSN) instead of glucose. The antibiotic concentrations used for *E. coli* were 100 $\mu\text{g}\cdot\text{ml}^{-1}$ ampicillin (Ap), 25 $\mu\text{g}\cdot\text{ml}^{-1}$ streptomycin (Sm), and 25 $\mu\text{g}\cdot\text{ml}^{-1}$ kanamycin (Km); for *A. tumefaciens*, they were 300 $\mu\text{g}\cdot\text{ml}^{-1}$ Km and 3 $\text{mg}\cdot\text{ml}^{-1}$ Sm. Media were supplemented with isopropylthio-beta-galactoside (IPTG) for P_{lac} induction. Reagents, antibiotics, and microbiological media were obtained from Fisher Scientific (Pittsburg, PA) and Sigma-Aldrich (St. Louis, MO).

Construction of complementation constructs. Complementation constructs were generated by cloning wild-type coding sequences into the IPTG-inducible expression vector pSRK-Km (59). For optimal gene expression, 5' primers were designed to fuse the NdeI site of pSRK-Km in frame with the *lacZ* α start codon. Coding sequences for the desired genes, i.e., wild-type *fliK*, Atu0572, *fliK*-Atu0572, and *motA* and their corre-

sponding *cms* mutant alleles, were PCR amplified with primers comp P1 and comp P2 from AtC58 genomic DNA or *cms* mutants using Phusion high-fidelity DNA polymerase. PCR fragments were gel purified and ligated to pGEM-T Easy, confirmed by sequencing, and then cleaved with the appropriate restriction enzymes to be religated to pSRK-Km, which was previously cleaved with the corresponding restriction enzymes. An *flgE* pPM110 expression plasmid (pBBR1-MCS-2 *P_{lac}::flgE*) from our previous study (24) was used as the source of the *flgE* gene, and this was ligated into pSRK-Km and electroporated into *A. tumefaciens* as described previously (56).

Construction of nonpolar markerless deletions. Nonpolar markerless deletions were constructed as described previously (24, 60). Briefly, about 500 to 1,000 bp of upstream and downstream DNA sequences flanking the desired gene were PCR amplified with P1 and P2 primers for the upstream sequence and with P3 and P4 primers for the downstream sequence. Primers were designed to delete a desired gene without affecting the adjacent genes, including any potential translational coupling in operons. Primers P2 and P3 for each gene were designed to have about 18 bp of homology (the overlap indicated in Table S2 in the supplemental material), enabling splicing by overlapping extension (SOEing) as described previously (24, 60, 61). The flanking sequences were amplified with Phusion high-fidelity DNA polymerase (NEB, Ipswich, MA), agarose gel purified, and used as the starting template and primer for a short, 5-cycle PCR. A final PCR round was performed using 2 μ l of the product of the above-described PCR as the template and primers P1 and P4 in order to fuse these flanking sequences. This resultant full-length product of about 1 kb was cloned into pGEM-T Easy (Promega, Madison, WI), confirmed by DNA sequencing, digested with the appropriate restriction enzymes, and ligated into the suicide vector pNPTS138, which was previously digested with the same set of enzymes. The pNPTS138 plasmid (62; M. R. K. Alley, unpublished data) confers Km resistance (Km^r) and sucrose sensitivity (Suc^s). pNPTS138 uses a ColE1 replication origin that does not function in *A. tumefaciens*, and thus, the plasmid must recombine into a stable endogenous replicon to impart the Km^r phenotype. Derivatives of pNPTS138 were introduced into *A. tumefaciens* by conjugation, and recombinants were selected for growth on ATGN Km plates. Km^r isolates were restreaked on ATGN Km plates and ATSN Km plates to confirm plasmid integration and sucrose sensitivity. Colonies with normal growth on ATGN Km plates and very poor growth on ATSN Km plates were selected. A single Km^r Suc^s colony was grown overnight in ATGN broth without antibiotic selection and then plated on ATSN to select for mutants that had excised the integrated plasmid via a second recombination event. The resultant Suc^c colonies were patched on ATSN and ATGN Km to verify plasmid excision. Primers P1 and P4 (the external primers designed to flank the targeted gene) were used to perform diagnostic PCR to identify recombinants in which the appropriate targeted gene was deleted. For construction of the $\Delta che \Delta flgE$ double mutant, a different suicide vector construct, pPM107, was used (Table S1). pPM107 is a pKNG101 suicide plasmid of R6K origin carrying the *flgE* SOE fragment. The derivatives of pKNG101 were introduced into the *A. tumefaciens* Δche mutant by mating using the protocol described above.

Allelic replacement of resident *A. tumefaciens* genes with the *cms* alleles. Allelic replacement of either the wild-type genes or preexisting *cms* mutant sequences with alleles carrying specific *cms* mutations in the wild type or the parent mutant background was performed using the same approach as with deletions. Primers were designed to amplify a fragment with the desired mutation in the center so as to facilitate efficient recombination events on each side of the mutation. Coding sequences for the targeted genes were PCR amplified with primers P1 *cms* and P2 *cms* from *cms* mutants *cms*-9, *cms*-2, and *cms*-3, respectively, using Phusion high-fidelity DNA polymerase. PCR fragments were gel purified and ligated to pGEM-T Easy, and the remainder of the procedure was identical to the protocol described above, including mating the pNPTS138::*cms* allele derivatives with the wild-type or appropriate parent mutant *A. tumefaciens*, up until the point of obtaining the desired Km^r/Suc^c colonies. DNA was

PCR amplified from these colonies using external sequencing primers flanking the desired gene. PCR fragments were gel purified, and the introduction of the appropriate *cms* mutation was confirmed via DNA sequencing using internal sequencing primers.

Site-directed mutagenesis for combining *cms* mutations. Site-directed mutagenesis was performed as described previously (62). The QuikChange protocol obtained from Stratagene Corp. was used to perform site-directed mutagenesis on the *cms*-5 (*flgE* Y127C) coding sequence. Long, self-complementary mutagenic primers *cms*-9 F1_{mut} and *cms*-9 R1_{mut} (melting temperature [T_m], $\sim 68^\circ\text{C}$) harboring the desired *cms*-9 mutation (*flgE* V93F) in the middle (underlined) were designed (GCAACGGTTTCTTCGTGGTTCAGGATGGGTCGGGC to GCAACGGTTTCTTCGTGTTTCAGGATGGGTCGGGC for Val to Phe) (see Table S2 in the supplemental material). pGEM-T Easy plasmid pRC103 containing the *cms*-5 mutation (Table S1) was used as a template to perform PCR with the mutagenic primers using Phusion DNA polymerase. The parental wild-type and hemimethylated plasmid DNA were removed by digesting the reaction products with DpnI, leaving only the newly synthesized, uniformly nonmethylated mutated DNA. DNA sequencing was performed to confirm the mutations, and then the mutated DNA fragment (the same *flgE* fragment, now harboring *cms*-5 Y127C and *cms*-9 V93F mutations) was used to mutagenize the *cms*-9 mutant by allelic replacement as described above.

Whole-genome sequencing of *cms* mutants. The *cms* suppressors obtained from motility agar flares were double-streak purified on ATGN. Total genomic DNA from the *cms* suppressor mutants was used to generate a paired-end library, following the modified protocol of Lazinski and Camilli (<http://tucf-genomics.tufts.edu/home/libraryprep>) as described in an earlier study (60). Approximately 20 μ g of sheared genomic DNA was blunt ended using the NEB Quick Blunting kit (New England Biolabs). The Klenow fragment of DNA polymerase I was used to add one deoxyadenosine to the 3' ends of the DNA preparation, and the DNA preparation was ligated with an adapter mix consisting of primers OLJ131 and OLJ137, using the NEB Quick Ligation kit (New England Biolabs). Finally, library amplification was performed by PCR with primers OLJ139 and OLJ140. Sequencing was performed on an Illumina HiSeq 2000 at the Tufts University Core Facility.

Motility assays. Flagellar swimming phenotypes were tested with ATGN motility (0.25 %) agar in 100-mm petri dishes with 20 ml of Bacto agar (BD, Sparks, MD), with the addition of Km and IPTG as necessary (63). Fresh colonies were used to inoculate swim plates, using a toothpick that was stabbed into the agar at the center of the plate. The plates were incubated at 28°C for up to 7 days, and their swim ring diameters were measured daily.

Cultivation and analysis of static-culture biofilms. For a static-culture biofilm assay, biofilms were grown as described previously (60, 64). Briefly, biofilms were grown on sterile polyvinyl chloride (PVC) coverslips placed vertically in the wells of UV-sterilized 12-well polystyrene cell culture plates (Corning, Inc.). Overnight bacterial cultures grown in ATGN were subcultured to an optical density at 600 nm (OD_{600}) of 0.2, grown at 28°C until exponential phase, and then diluted to an OD_{600} of 0.05 in about 3 ml of ATGN, followed by 48 h of room temperature incubation. Coverslips were removed, rinsed with water, and stained with 0.1% (wt/vol) crystal violet (CV) for 5 to 7 min. The coverslips were further washed with water to remove excess stain. Coverslip biofilms were soaked in 1 ml of 33% acetic acid to solubilize the CV stain, and the absorbance at 600 nm (A_{600}) was measured in a Bio-Tek Synergy HT microplate reader. The A_{600} value of solubilized CV was normalized to the OD_{600} of the planktonic cells to obtain the A_{600}/OD_{600} ratio, and this ratio was normalized to the wild type or parent mutant value as appropriate.

Transmission electron microscopy. Transmission electron microscopy was performed as described previously with a few modifications (65). *A. tumefaciens* cells were grown in appropriate medium (ATGN) to an OD_{600} of ≈ 1.0 and were diluted 1:10 before being used to coat 300-mesh, 3-mm copper grids with carbon-formvar films for 5 min (Electron Microscopy Sciences, Hatfield, PA). Each grid was dried with filter paper

and then negatively stained with 2% uranyl acetate for another 5 min. The grids were dried to remove excess stain and then examined with a JEOL JEM-1010 transmission electron microscope set to 80 kV in the Indiana University Electron Microscopy Center.

Sequence comparisons and threading of class I cms mutations through the *Salmonella* hook crystal structure. The amino acid sequences of *A. tumefaciens* and *S. Typhimurium* FlgE were compared via BLASTp analysis (66). The FASTA *A. tumefaciens* and *S. Typhimurium* FlgE and *A. tumefaciens* and *E. coli* MotA amino acid sequences were imported from the PubMed Protein database to Clustal Omega and aligned using the default settings (31). The class I cms mutations were mapped to the hook structure as described in detail above (see Results, “Class I cms mutations map to the FlgE D1 domain”).

Tracking swimming behavior of the bacteria. Overnight bacterial cultures of *A. tumefaciens* cells grown in ATGN were subcultured to mid-exponential phase. Swimming movies were captured using a 10× dark-field objective on a Nikon 90i microscope. Movies were captured with an exposure of 30 ms and frame duration of 0.03283 s. The movies were each ~10.6 s long. The raw files were imported into the Fiji image analysis package and processed with the Mosaic two-dimensional single-particle tracking tool plug-in to track the individual cells; only trajectories longer than 40 frames were analyzed further, and a trajectory report was generated (39, 40). Twenty separate single-cell trajectories (of at least 50 μm in length) obtained for each strain were analyzed to calculate their reorientation frequencies over time and their swimming speed. The trajectory report obtained from the Mosaic particle tracker plug-in was used to calculate the length, time scale, and swimming speed from the trajectories. Trajectory reports were then imported into MatLab version 8.1.0.604 (67) to obtain trajectory plots. The number of reorientations made by a single cell over time was counted by eye from the traces. Trajectories are plotted as a square plot centered around 0. Box plots are used (Fig. 6F and G) to indicate the speed and reorientation frequencies of swimming cells. Reorientations are expressed per second and are only counted if they changed the overall direction of the cell; i.e., jittery swimming that maintained the basic trajectory is not considered a reorientation. The swimming speed is in micrometers per second and includes times when cells were actively tumbling. Evaluation of the swimming speeds that did not include the reorientation periods revealed the same basic trend that the class III mutant was slower than the wild type and the other cms mutants.

SUPPLEMENTAL MATERIAL

Supplemental material for this article may be found at <http://mbio.asm.org/lookup/suppl/doi:10.1128/mBio.00005-15/-DCSupplemental>.

- Figure S1, PDF file, 0.6 MB.
- Figure S2, PDF file, 0.5 MB.
- Figure S3, PDF file, 0.7 MB.
- Figure S4, PDF file, 1 MB.
- Figure S5, PDF file, 0.5 MB.
- Table S1, PDF file, 0.1 MB.
- Table S2, PDF file, 0.1 MB.

ACKNOWLEDGMENTS

This work was supported by National Institutes of Health grants R01 GM080546 (C.F.) and R01 GM051986 (Y.V.B.) and by National Science Foundation award PHY-0645652 (S.S.). DTK was supported by National Institutes of Health National Research Service award GM083581. We thank Birgit Scharf, Gladys Alexandre, and Kelly Hughes for helpful comments on the manuscript.

REFERENCES

1. Berg HC. 2003. The rotary motor of bacterial flagella. *Annu Rev Biochem* 72:19–54. <http://dx.doi.org/10.1146/annurev.biochem.72.121801.161737>.
2. Kubori T, Shimamoto N, Yamaguchi S, Namba K, Aizawa S. 1992. Morphological pathway of flagellar assembly in *Salmonella typhimurium*. *J Mol Biol* 226:433–446. [http://dx.doi.org/10.1016/0022-2836\(92\)90958-M](http://dx.doi.org/10.1016/0022-2836(92)90958-M).
3. Scharf B. 2002. Real-time imaging of fluorescent flagellar filaments of *Rhizobium lupini* H13-3: flagellar rotation and pH-induced polymorphic transitions. *J Bacteriol* 184:5979–5986. <http://dx.doi.org/10.1128/JB.184.21.5979-5986.2002>.
4. Götz R, Schmitt R. 1987. *Rhizobium meliloti* swims by unidirectional, intermittent rotation of right-handed flagellator helices. *J Bacteriol* 169:3146–3150.
5. Attmannspacher U, Scharf B, Schmitt R. 2005. Control of speed modulation (chemokinesis) in the unidirectional rotary motor of *Sinorhizobium meliloti*. *Mol Microbiol* 56:708–718. <http://dx.doi.org/10.1111/j.1365-2958.2005.04565.x>.
6. Berg HC, Brown DA. 1972. Chemotaxis in *Escherichia coli* analyzed by 3-dimensional tracking. *Nature* 239:500–504. <http://dx.doi.org/10.1038/239500a0>.
7. Reigh SY, Winkler RG, Gompper G. 2013. Synchronization, slippage, and unbundling of driven helical flagella. *PLoS One* 8:e70868. <http://dx.doi.org/10.1371/journal.pone.0070868>.
8. Berg HC. 2004. *E. coli* in motion. Springer-Verlag, New York, NY.
9. Dyer CM, Vartanian AS, Zhou H, Dahlquist FW. 2009. A molecular mechanism of bacterial flagellar motor switching. *J Mol Biol* 388:71–84. <http://dx.doi.org/10.1016/j.jmb.2009.02.004>.
10. Paul K, Brunstetter D, Titen S, Blair DF. 2011. A molecular mechanism of direction switching in the flagellar motor of *Escherichia coli*. *Proc Natl Acad Sci U S A* 108:17171–17176. <http://dx.doi.org/10.1073/pnas.1110111108>.
11. Morimoto YV, Nakamura S, Hiraoka KD, Namba K, Minamino T. 2013. Distinct roles of highly conserved charged residues at the MotA-Flig interface in bacterial flagellar motor rotation. *J Bacteriol* 195:474–481. <http://dx.doi.org/10.1128/JB.01971-12>.
12. Adler J. 1969. Chemoreceptors in bacteria. *Science* 166:1588–1597. <http://dx.doi.org/10.1126/science.166.3913.1588>.
13. Armstrong JB, Adler J. 1969. Location of genes for motility and chemotaxis on the *Escherichia coli* genetic map. *J Bacteriol* 97:156–161.
14. Adler J. 1973. Method for measuring chemotaxis and use of the method to determine optimum conditions for chemotaxis by *Escherichia coli*. *J Gen Microbiol* 74:77–91. <http://dx.doi.org/10.1099/00221287-74-1-77>.
15. Adler J. 1976. Chemotaxis in bacteria. *J Supramol Struct* 4:305–317. <http://dx.doi.org/10.1002/jss.400040302>.
16. Parkinson JS, Parker SR, Talbert PB, Houts SE. 1983. Interactions between chemotaxis genes and flagellar genes in *Escherichia coli*. *J Bacteriol* 155:265–274.
17. Yonekawa H, Hayashi H, Parkinson JS. 1983. Requirement of the CheB function for sensory adaptation in *Escherichia coli*. *J Bacteriol* 156:1228–1235.
18. Alon U, Camarena L, Surette MG, Aguera y Arcas B, Liu Y, Leibler S, Stock JB. 1998. Response regulator output in bacterial chemotaxis. *EMBO J* 17:4238–4248. <http://dx.doi.org/10.1093/emboj/17.15.4238>.
19. Parkinson JS. 1978. Complementation analysis and deletion mapping of *Escherichia coli* mutants defective in chemotaxis. *J Bacteriol* 135:45–53.
20. Parkinson JS, Houts SE. 1982. Isolation and behavior of *Escherichia coli* deletion mutants lacking chemotaxis functions. *J Bacteriol* 151:106–113.
21. Wolfe AJ, Berg HC. 1989. Migration of bacteria in semisolid agar. *Proc Natl Acad Sci U S A* 86:6973–6977. <http://dx.doi.org/10.1073/pnas.86.18.6973>.
22. Magariyama Y, Yamaguchi S, Aizawa S. 1990. Genetic and behavioral analysis of flagellar switch mutants of *Salmonella typhimurium*. *J Bacteriol* 172:4359–4369.
23. Sockett H, Yamaguchi S, Kihara M, Irikura VM, Macnab RM. 1992. Molecular analysis of the flagellar switch protein FlhM of *Salmonella typhimurium*. *J Bacteriol* 174:793–806.
24. Merritt PM, Danhorn T, Fuqua C. 2007. Motility and chemotaxis in *Agrobacterium tumefaciens* surface attachment and biofilm formation. *J Bacteriol* 189:8005–8014. <http://dx.doi.org/10.1128/JB.00566-07>.
25. Chesnokova O, Coutinho JB, Khan IH, Mikhail MS, Kado CI. 1997. Characterization of flagella genes of *Agrobacterium tumefaciens*, and the effect of a bald strain on virulence. *Mol Microbiol* 23:579–590. <http://dx.doi.org/10.1046/j.1365-2958.1997.d01-1875.x>.
26. Loake GJ, Ashby AM, Shaw CH. 1988. Attraction of *Agrobacterium tumefaciens* C58C1 towards sugars involves a highly sensitive chemotaxis system. *J Gen Microbiol* 134:1427–1432. <http://dx.doi.org/10.1099/00221287-134-6-1427>.
27. Götz R, Limmer N, Ober K, Schmitt R. 1982. Motility and chemotaxis in 2 strains of *Rhizobium* with complex flagella. *J Gen Microbiol* 128:789–798.

28. Armitage JP, Schmitt R. 1997. Bacterial chemotaxis: *Rhodobacter sphaeroides* and *Sinorhizobium meliloti*—variations on a theme? *Microbiology* 143:3671–3682. <http://dx.doi.org/10.1099/00221287-143-12-3671>.
29. Fujii T, Kato T, Namba K. 2009. Specific arrangement of alpha-helical coiled coils in the core domain of the bacterial flagellar hook for the universal joint function. *Structure* 17:1485–1493. <http://dx.doi.org/10.1016/j.str.2009.08.017>.
30. Samatey FA, Matsunami H, Imada K, Nagashima S, Shaikh TR, Thomas DR, Chen JZ, DeRosier DJ, Kitao A, Namba K. 2004. Structure of the bacterial flagellar hook and implication for the molecular universal joint mechanism. *Nature* 431:1062–1068. <http://dx.doi.org/10.1038/nature02997>.
31. Sievers F, Wilm A, Dineen D, Gibson TJ, Karplus K, Li W, Lopez R, McWilliam H, Remmert M, Söding J, Thompson JD, Higgins DG. 2011. Fast, scalable generation of high-quality protein multiple sequence alignments using Clustal Omega. *Mol Syst Biol* 7:539. <http://dx.doi.org/10.1038/msb.2011.1075>.
32. Schrödinger L. The PyMOL molecular graphics system, version 1504.
33. Huang CC, Couch GS, Pettersen EF, Ferrin TE. 1996. Chimera: an extensible molecular modeling application constructed using standard components. *Pac Symp Biocomput* 1:724.
34. Furuta T, Samatey FA, Matsunami H, Imada K, Namba K, Kitao A. 2007. Gap compression/extension mechanism of bacterial flagellar hook as the molecular universal joint. *J Struct Biol* 157:481–490. <http://dx.doi.org/10.1016/j.jmb.2006.10.006>.
35. Brown MT, Steel BC, Silvestrin C, Wilkinson DA, Delalez NJ, Lumb CN, Obara B, Armitage JP, Berry RM. 2012. Flagellar hook flexibility is essential for bundle formation in swimming *Escherichia coli* cells. *J Bacteriol* 194:3495–3501. <http://dx.doi.org/10.1128/JB.00209-12>.
36. Shaikh TR, Thomas DR, Chen JZ, Samatey FA, Matsunami H, Imada K, Namba K, DeRosier DJ. 2005. A partial atomic structure for the flagellar hook of *Salmonella typhimurium*. *Proc Natl Acad Sci U S A* 102:1023–1028. <http://dx.doi.org/10.1073/pnas.0409020102>.
37. Eggenhofer E, Rachel R, Haslbeck M, Scharf B. 2006. MotD of *Sinorhizobium meliloti* and related alpha-proteobacteria is the flagellar-hook-length regulator and therefore reassigned as FliK. *J Bacteriol* 188:2144–2153. <http://dx.doi.org/10.1128/JB.188.6.2144-2153.2006>.
38. Erhardt M, Singer HM, Wee DH, Keener JP, Hughes KT. 2011. An infrequent molecular ruler controls flagellar hook length in *Salmonella enterica*. *EMBO J* 30:2948–2961. <http://dx.doi.org/10.1038/emboj.2011.185>.
39. Sbalzarini IF, Koumoutsakos P. 2005. Feature point tracking and trajectory analysis for video imaging in cell biology. *J Struct Biol* 151:182–195. <http://dx.doi.org/10.1016/j.jmb.2005.06.002>.
40. Schindelin J, Arganda-Carreras I, Frise E, Kaynig V, Longair M, Pietzsch T, Preibisch S, Rueden C, Saalfeld S, Schmid B, Tinevez JY, White DJ, Hartenstein V, Eliceiri K, Tomancak P, Cardona A. 2012. Fiji: an open-source platform for biological-image analysis. *Nat Methods* 9:676–682. <http://dx.doi.org/10.1038/nmeth.2019>.
41. Serrano L, Neira JL, Sancho J, Fersht AR. 1992. Effect of alanine versus glycine in alpha-helices on protein stability. *Nature* 356:453–455. <http://dx.doi.org/10.1038/356453a0>.
42. Reigh SY, Winkler RG, Gompper G. 2012. Synchronization and bundling of anchored bacterial flagella. *Soft Matter* 8:4363–4372. <http://dx.doi.org/10.1039/c2sm07378a>.
43. Lele PP, Hosu BG, Berg HC. 2013. Dynamics of mechanosensing in the bacterial flagellar motor. *Proc Natl Acad Sci U S A* 110:11839–11844. <http://dx.doi.org/10.1073/pnas.1305885110>.
44. Schmitt R, Bamberger I, Acker G, Mayer F. 1974. Fine structure analysis of the complex flagella of *Rhizobium lupini* H13-3. *Arch Microbiol* 100:145–162. <http://dx.doi.org/10.1007/BF00446314>.
45. Yen JY, Broadway KM, Scharf BE. 2012. Minimum requirements of flagellation and motility for infection of *Agrobacterium* sp. strain H13-3 by flagellotropic bacteriophage 7-7-1. *Appl Environ Microbiol* 78:7216–7222. <http://dx.doi.org/10.1128/AEM.01082-12>.
46. Sourjik V, Schmitt R. 1996. Different roles of CheY1 and CheY2 in the chemotaxis of *Rhizobium meliloti*. *Mol Microbiol* 22:427–436. <http://dx.doi.org/10.1046/j.1365-2958.1996.1291489.x>.
47. Greck M, Platzer J, Sourjik V, Schmitt R. 1995. Analysis of a chemotaxis operon in *Rhizobium meliloti*. *Mol Microbiol* 15:989–1000. <http://dx.doi.org/10.1111/j.1365-2958.1995.tb02274.x>.
48. Vladimirov N, Løvdok L, Lebedz D, Sourjik V. 2008. Dependence of bacterial chemotaxis on gradient shape and adaptation rate. *PLoS Comput Biol* 4:e1000242. <http://dx.doi.org/10.1371/journal.pcbi.1000242>.
49. Wadhams GH, Armitage JP. 2004. Making sense of it all: bacterial chemotaxis. *Nat Rev Mol Cell Biol* 5:1024–1037. <http://dx.doi.org/10.1038/nrm1524>.
50. Faguy DM, Jarrell KF. 1999. A twisted tale: the origin and evolution of motility and chemotaxis in prokaryotes. *Microbiology* 145:279–281. <http://dx.doi.org/10.1099/13500872-145-2-279>.
51. Gode-Potratz CJ, Kustusch RJ, Breheny PJ, Weiss DS, McCarter LL. 2011. Surface sensing in *Vibrio parahaemolyticus* triggers a programme of gene expression that promotes colonization and virulence. *Mol Microbiol* 79:240–263. <http://dx.doi.org/10.1111/j.1365-2958.2010.07445.x>.
52. Li G, Brown PJ, Tang JX, Xu J, Quardokus EM, Fuqua C, Brun YV. 2012. Surface contact stimulates the just-in-time deployment of bacterial adhesins. *Mol Microbiol* 83:41–51. <http://dx.doi.org/10.1111/j.1365-2958.2011.07909.x>.
53. Frymier PD, Ford RM, Berg HC, Cummings PT. 1995. Three dimensional tracking of motile bacteria near a solid planar surface. *Proc Natl Acad Sci U S A* 92:6195–6199. <http://dx.doi.org/10.1073/pnas.92.13.6195>.
54. Kirov SM, Castrisios M, Shaw JG. 2004. *Aeromonas* flagella (polar and lateral) are enterocyte adhesins that contribute to biofilm formation on surfaces. *Infect Immun* 72:1939–1945. <http://dx.doi.org/10.1128/IAI.72.4.1939-1945.2004>.
55. Sambrook J, Fritsch E, Maniatis T. 1989. *Molecular cloning: a laboratory manual*. Cold Spring Harbor Laboratory Press, Cold Spring Harbor, NY.
56. Mersereau M, Pazour GJ, Das A. 1990. Efficient transformation of *Agrobacterium tumefaciens* by electroporation. *Gene* 90:149–151. [http://dx.doi.org/10.1016/0378-1119\(90\)90452-W](http://dx.doi.org/10.1016/0378-1119(90)90452-W).
57. Fuqua WC, Winans SC. 1994. A LuxR-LuxI type regulatory system activates *Agrobacterium* Ti plasmid conjugal transfer in the presence of a plant tumor metabolite. *J Bacteriol* 176:2796–2806.
58. Tempé J, Petit A, Holsters M, Montagu M, Schell J. 1977. Thermosensitive step associated with transfer of Ti plasmid during conjugation—possible relation to transformation in crown gall. *Proc Natl Acad Sci U S A* 74:2848–2849. <http://dx.doi.org/10.1073/pnas.74.7.2848>.
59. Khan SR, Gaines J, Roop RM, Farrand SK. 2008. Broad-host-range expression vectors with tightly regulated promoters and their use to examine the influence of TraR and TraM expression on Ti plasmid quorum sensing. *Appl Environ Microbiol* 74:5053–5062. <http://dx.doi.org/10.1128/AEM.01098-08>.
60. Kim J, Heindl JE, Fuqua C. 2013. Coordination of division and development influences complex multicellular behavior in *Agrobacterium tumefaciens*. *PLoS One* 8:e56682. <http://dx.doi.org/10.1371/journal.pone.0056682>.
61. Warrens AN, Jones MD, Lechler RI. 1997. Splicing by overlap extension by PCR using asymmetric amplification: an improved technique for the generation of hybrid proteins of immunological interest. *Gene* 186:29–35. [http://dx.doi.org/10.1016/S0378-1119\(96\)00674-9](http://dx.doi.org/10.1016/S0378-1119(96)00674-9).
62. Hibbing ME, Fuqua C. 2011. Antiparallel and interlinked control of cellular iron levels by the Irr and RirA regulators of *Agrobacterium tumefaciens*. *J Bacteriol* 193:3461–3472. <http://dx.doi.org/10.1128/JB.00317-11>.
63. Adler J. 1966. Chemotaxis in bacteria. *Science* 153:708–716. <http://dx.doi.org/10.1126/science.153.3737.708>.
64. Ramey BE, Matthyse AG, Fuqua C. 2004. The FNR-type transcriptional regulator SinR controls maturation of *Agrobacterium tumefaciens* biofilms. *Mol Microbiol* 52:1495–1511. <http://dx.doi.org/10.1111/j.1365-2958.2004.04079.x>.
65. Wang Y, Haitjema CH, Fuqua C. 2014. The Ctp type IVb pilus locus of *Agrobacterium tumefaciens* directs formation of the common pili and contributes to reversible surface attachment. *J Bacteriol* 196:2979–2988. <http://dx.doi.org/10.1128/JB.01670-14>.
66. Altschul SF, Gish W, Miller W, Myers EW, Lipman DJ. 1990. Basic local alignment search tool. *J Mol Biol* 215:403–410. [http://dx.doi.org/10.1016/S0022-2836\(05\)80360-2](http://dx.doi.org/10.1016/S0022-2836(05)80360-2).
67. MathWorks. 2013. MatLab version 8.1.0.604 (R2013a). MathWorks, Natick, MA.
68. Uedaira H, Morii H, Ishimura M, Taniguchi H, Namba K, Vonderviszt F. 1999. Domain organization of flagellar hook protein from *Salmonella typhimurium*. *FEBS Lett* 445:126–130. [http://dx.doi.org/10.1016/S0014-5793\(99\)00110-6](http://dx.doi.org/10.1016/S0014-5793(99)00110-6).